Flanking Sequence Specificity Determines Coding Microsatellite Heteroduplex and Mutation Rates with Defective DNA Mismatch Repair (MMR)

Heekyung Chung[*], **Claudia G. Lopez**[*], **Dennis J. Young**[§], **Jenny F. Lai**[*], **Joy Holmstrom**[*], **Deena Ream-Robinson**[*], **Betty L. Cabrera**[*], and **John M. Carethers**[*,§,#]

[*]Department of Medicine, University of California, San Diego, California

[§]Rebecca and John Moores Comprehensive Cancer Center, University of California, San Diego, California

[#]VA San Diego Healthcare System, San Diego, California

Abstract

The *activin type II receptor* (*ACVR2*) contains 2 identical microsatellites in exon 3 and 10, but only the exon 10 microsatellite is frameshifted in MMR-defective colonic tumors. The reason for this selectivity is not known. We hypothesized that *ACVR2* frameshifts were influenced by DNA sequences surrounding the microsatellite. We constructed plasmids in which exon 3 or 10 of *ACVR2* were cloned +1bp out-of-frame of EGFP, allowing −1bp frameshift to express EGFP. Plasmids were stably-transfected into MMR-deficient cells, subsequent non-fluorescent cells sorted, cultured, and harvested for mutation analysis. We swapped DNA sequences flanking the exon 3 and 10 microsatellites to test our hypothesis. Native *ACVR2* exon 3 and 10 microsatellites underwent heteroduplex formation (A_7/T_8) in *hMLH1*$^{-/-}$ cells, but only exon 10 microsatellites fully mutated (A_7/T_7) in both *hMLH1*$^{-/-}$ and *hMSH6*$^{-/-}$ backgrounds, showing selectivity for exon 10 frameshifts and inability of exon 3 heteroduplexes to fully mutate. Substituting nucleotides flanking the exon 3 microsatellite for nucleotides flanking the exon 10 microsatellite significantly reduced heteroduplex and full mutation in *hMLH1*$^{-/-}$ cells. When the exon 3 microsatellite was flanked by nucleotides normally surrounding the exon 10 microsatellite, fully-mutant exon 3 frameshifts appeared. Mutation selectivity for *ACVR2* lies partly with flanking nucleotides surrounding each microsatellite.

Corresponding author: John M. Carethers, M.D., University of California San Diego, Univ. Center 303, MC0063, 9500 Gilman Drive, La Jolla, CA 92093, Phone: (858) 534-3320, Fax: (858) 534-3338., jcarethers@ucsd.edu.
New address (as of November 1, 2009): John M. Carethers, M.D., Department of Internal Medicine, 3101 Taubman Center, University of Michigan, 1500 East Medical Center Drive, Ann Arbor, MI, 48109, jcarethe@umich.edu

Keywords

ACVR2; microsatellite; frameshift mutation; MMR; Microsatellite instability; colonic tumors

INTRODUCTION

Functional human DNA MMR activity requires hMutSα (a heterodimer of hMSH2 and hMSH6) and hMutSβ (a heterodimer of hMSH2 and hMSH3) to recognize and bind mispairs and/or insertion/deletion loops (IDLs) that occur at microsatellite sequences, and hMutLα (a heterodimer of hMLH1 and hPMS2) to help coordinate DNA repair (Acharya et al., 1996; Palombo et al., 1996). More specifically, hMutSα recognizes single nucleotide interstrand mispairs and IDLs containing 1 or 2 looped nucleotides, whereas hMutSβ recognizes IDLs of 2 nucleotides or more (Modrich, 2006). Subsequently, the hMutSα or hMutSβ heterodimer interacts with the hMutLα complex to coordinate excision and repair of the mispair or IDL (Modrich, 2006). Defects in DNA MMR cause microsatellite instability (MSI) due to the inability of the system to recognize or repair frameshifts at the microsatellites (Grady & Carethers, 2008). Germline mutations of *hMSH2*, *hMLH1*, *hMSH6*, or *hPMS2* cause Lynch syndrome, which has an 80% lifetime risk for colorectal cancer (CRC), and epigenetic inactivation of *hMLH1* by promoter hypermethylation is seen in 15–20% of sporadic CRC (Akiyama et al., 1997; Fishel et al., 1993; Herman et al., 1998; Nicolaides et al., 1994; Papadopoulos et al., 1994; Veigl et al., 1998). CRC from Lynch syndrome and sporadic *hMLH1* defective cancer patients display the phenotype of MSI (Grady & Carethers, 2008).

Microsatellite sequences are predominantly located in the non-coding regions of the genome (Thibodeau et al., 1993). However, some microsatellites are present in the exonic coding regions of genes, with accumulation of frameshift mutation within alleles of these genes deregulating normal cellular processes and driving the pathogenesis of CRC with MSI (Jung et al., 2006; Woerner et al., 2005). An A_{10} microsatellite within the transforming growth factor β receptor 2 (*TGFBR2*) exon 3 and an A_8 microsatellite within *ACVR2* exon 10 become −1bp frameshift mutated at both alleles in 70–90% of CRC with MSI (Hempen et al., 2003; Jung et al., 2004; Parsons et al., 1995). These frameshift mutations of *TGFBR2* and *ACVR2* cause loss of protein expression and their growth suppressive effects that are mediated by intracellular SMAD signaling (Jung et al., 2006; Markowitz et al., 1995). Furthermore, we have measured the mutation rates of *TGFBR2* exon 3 and *ACVR2* exon 10 and shown that both accumulate frameshift mutations in *hMLH1*-defective and *hMSH6*-defective cells after forming heteroduplexes at a constant rate of formation (Chung et al., 2008).

ACVR2 shows exonic selectivity for frameshift mutation. *ACVR2* contains identical octoadenine tracts in exon 3 and 10, but only its exon 10 octoadenine tract is mutated in CRC with MSI (Hempen et al., 2003; Jung et al., 2004). The cause for this selectivity is not known, although this is an important concept that potentially drives the pathogenesis of CRC and may determine which genes and coding microsatellites become mutated. The spectra of genes with coding microsatellites are broad but appear to favor tumor suppressors;

however, the frequency for mutation of genes is varied in cancers, even when microsatellite lengths are identical. The two identical intragenic *ACVR2* microsatellites afforded us an opportunity to accurately measure mutation rates, plus manipulate the sequences surrounding the microsatellite to test the hypothesis that the primary DNA sequence influences microsatellite mutation. In yeast models, it was reported that the 6 nucleotides surrounding mispair influence mispair recognition by MMR proteins and may alter mutation rates (Marsischky & Kolodner, 1999). To study this in a human model, we constructed EGFP plasmids in which a −1 bp frameshift mutation at the coding microsatellites of *ACVR2* exon 10 and 3 could be detected by EGFP expression in MMR deficient cells. We also swapped the DNA sequences surrounding exon 10 and 3 microsatellites of *ACVR2* to determine if this modifies frameshift mutation rates. Observed in real time, we demonstrate exonic selectivity of *ACVR2* exon 10 for frameshift mutation over *ACVR2* exon 3 with MMR deficiency, and further demonstrate that DNA sequences flanking the exon 3 and 10 microsatellites of *ACVR2* alter frameshift mutation.

MATERIALS AND METHODS

Cloning of pIREShyg2-ACVR2 exon 10-EGFP and pIREShyg2-ACVR2 exon 3-EGFP plasmids

Plasmids pIREShyg2-ACVR2 exon 10-EGFP, containing portions of exon 10 of *hACVR2* were constructed previously (Chung et al., 2008). Details of plasmid cloning were previously described (Chung et al., 2008) and the same cloning strategies were used to construct plasmids pIREShyg2-ACVR2 exon 3-EGFP containing portions of exon 3 of *hACVR2*. Briefly, portions of exon 10 or 3 of *ACVR2* (Table 1) were inserted immediately after the start codon of the EGFP gene, either in-frame of EGFP (IF) or +1 bp out of frame of EGFP (OF) in pIREShyg2-EGFP. For experimental plasmids, *ACVR2* sequences were cloned +1 bp OF in pIREShyg2-EGFP and thus a −1bp frameshift mutation at the coding microsatellite would allow EGFP expression. Mutation resistant (MR) counterpart plasmids were constructed by interrupting the microsatellites (A_8 to A_3GA_4) using a Quickchange II site-directed mutagenesis kit (Stratagene, La Jolla, CA). The MR *ACVR2* plasmids were placed OF (+1bp) and IF to be used as negative and positive controls for EGFP expression, respectively.

Cloning of pIREShyg2-ACVR2 exon 10-exon 3 Flanking (F)-EGFP and pIREShyg2-ACVR2 exon 3-exon 10 F-EGFP plasmids

Plasmids pIREShyg2-*ACVR2* exon 10-exon 3 F OF and pIREShyg2-*ACVR2* exon 3-exon 10 F OF (named as substituted plasmids) were constructed in which six nucleotides flanking *ACVR2* exons 10 or 3 microsatellites on the 5′ and 3′ ends were replaced with the 6 nucleotides flanking *ACVR2* exons 3 or 10 microsatellites by a site-directed mutagenesis, respectively (Table 1). MR-IF plasmids for each substituted ACVR2 plasmid were constructed (Table 1).

Cell lines, transfection, and selection

The human colon cancer cell lines, HCT116 (*hMLH1*^{−/−} and *hMSH3*^{−/−}), DLD-1 (*hMSH6*^{−/−}), and HCT116+chr3 (*hMLH1* restored but *hMSH3*^{−/−}) were cultured as

described previously (Chung et al., 2008). Cells were transfected with the different pIREShyg2-ACVR2-EGFP plasmids (described in Table 1) by using Nucleofector kits (Amaxa, Cologne, Germany) and stable cell lines were generated by hygromycin B (Invitrogen Corp, Carlsbad, CA) selection. After selection, colonies from each cell line were initially pooled and cultured for mutation analysis. All stable cell lines were confirmed by DNA sequencing.

Mutation Analysis by flow cytometry

Details of analysis of mutant cells by flow cytometry were previously described (Chung et al., 2008). Briefly, five thousand non-fluorescent cells expressing MR *ACVR2* exon 10 OF, *ACVR2* exon 10 OF, *ACVR2* exon 10-exon 3 F OF, MR *ACVR2* exon 3 OF, *ACVR2* exon 3 OF, or *ACVR2* exon 3-exon 10 F OF were sorted into 24-well plates by FACS ARIA (Becton Dickinson, San Jose, CA). During the analysis period, cultures were expanded as required to keep cells in exponential growth. Cells were trypsinized, washed in PBS, and resuspended in a total volume of 200 μl of PBS/ 0.5 μg/ml of propidium iodide (PI) and 3% BSA. At specified time points, Cell suspensions from two cultures were analyzed in parallel on a FACSCalibur (Becton Dickinson). The population with dim EGFP fluorescence was designated M1, and the population with bright EGFP fluorescence was designated M2. The counts of M1 and M2 cells were expressed as percentages of total live cell number.

PCR and DNA sequencing

Total cellular DNA from stable cell lines as well as M1 and M2 cell populations were PCR-amplified by specific primers (Fig. S2) using a cloned *Pfu* DNA polymerase (Stratagene). The PCR products were used for DNA sequencing to identify stable cell lines and frameshift mutations at microsatellites of *ACVR2* exon 10 and 3. Additionally, we subcloned PCR-amplified *ACVR2* DNA fragments from the M1 and M2 cell populations by utilizing a TA cloning vector (Invitrogen Corp) as per the manufacturer's protocol. DNA clones were then individually sequenced to determine the prevalence of mutated and WT *ACVR2* microsatellite sequences.

Determination of –1 bp frameshift mutation rates of *ACVR2* sequences in MMR-deficient cells

Mutation rates were calculated by the "method of the mean" developed by Luria and Delbruck (Luria & Delbruck, 1943) as described previously (Chung et al., 2008).

Statistical analysis

Mutation frequencies and rates of cell lines were compared by T-test or one-way ANOVA.

RESULTS

Selectivity for frameshift mutation of *ACVR2* exon 10 over *ACVR2* exon 3, and dependence on the DNA MMR background

To measure the exonic selectivity of *ACVR2* for frameshift mutation, we utilized stable cell lines containing native *ACVR2* exon 10 or 3 sequences within *hMLH1*$^{-/-}$, *hMSH6*$^{-/-}$, and

hMSH3$^{-/-}$ backgrounds (Table S1). At 4 weeks after establishing stable cell lines, the proportion for fluorescent cells within each cell line was measured by flow cytometry. All MR *ACVR2* IF cell lines showed fluorescence between 83 and 100 % (median 96%), demonstrating robust EGFP expressional selection efficiency. The *hMLH1*$^{-/-}$ *ACVR2* exon 10 and *ACVR2* exon 3 OF cells, and *hMSH6*$^{-/-}$ *ACVR2* exon 10 OF cells revealed newly fluorescent cells ranging between 0.10% and 0.72% (median 0.13%) net fluorescence over counterpart MR *ACVR2* exon 10 OF or MR *ACVR2* exon 3 OF cells. The *hMLH1*$^{-/-}$ *ACVR2* exon 10 OF cells showed the highest net fluorescence (0.72%) among all stable cell lines. *hMSH6*$^{-/-}$ *ACVR2* exon 3 OF cells and all *hMSH3*$^{-/-}$ stable cell lines did not show any net EGFP fluorescence.

To establish mutation frequencies of the *ACVR2* exon 10 and 3 coding microsatellites in cells with different MMR backgrounds (Table S1), non-fluorescent cells (i.e. cells without baseline mutation) containing either MR *ACVR2* exon 10 OF, *ACVR2* exon 10 OF, MR *ACVR2* exon 3 OF or *ACVR2* exon 3 OF were sorted and exponentially grown for 7 to 28 days. EGFP flow cytometric histograms at day 21 were shown in Fig. 1. As we observed previously (Chung et al., 2008), two distinct EGFP expressing cell populations, M1 and M2 were revealed from *hMLH1*$^{-/-}$ *ACVR2* exon 10 OF cells. However, no significant proportion of the M2 population was observed in *hMLH1*$^{-/-}$ *ACVR2* exon 3 OF cells. Additionally, *hMSH6*$^{-/-}$ *ACVR2* exon 3 OF cells revealed only an M1 population whereas *hMSH6*$^{-/-}$ *ACVR2* exon 10 OF revealed both M1 and M2 populations. These findings indicate selectivity for *ACVR2* exon 10 mutation in *hMLH1*$^{-/-}$ and *hMSH6*$^{-/-}$ backgrounds, with lack of development of *ACVR2* exon 3 mutation in the same MMR-deficient backgrounds.

We performed sequencing analysis to confirm that fluorescence from the M1 and M2 populations was driven by −1 bp frameshift mutation. At day 21 after plating non-fluorescent cells, the M1 and/or M2 cell populations of MR *ACVR2* exon 10 OF, *ACVR2* exon 10 OF, MR *ACVR2* exon 3 OF, and *ACVR2* exon 3 OF from the different MMR deficient backgrounds were sorted and expanded for sequencing analysis (Fig. 2). The M2 populations of *ACVR2* exon 10 OF cell lines in *hMLH1*$^{-/-}$ and *hMSH6*$^{-/-}$ backgrounds revealed only −1 bp frameshifted microsatellite sequence (A_7), indicating full mutant (A_7/T_7) formation that induces bright EGFP expression as observed previously (Chung et al., 2008). In comparison, the M1 populations of *hMLH1*$^{-/-}$ *ACVR2* exon 10 OF and *ACVR2* exon 3 OF cells revealed overlapping sequences, with WT and mutant microsatellite sequences present, highly suggestive of heteroduplex (A_7/T_8) formation that weakly drives EGFP expression (Chung et al., 2008). The M1 cells from *hMLH1*$^{-/-}$ *ACVR2* exon 10 OF revealed a higher proportion of mutant sequence (the main peak is A_7) compared to *hMLH1*$^{-/-}$ *ACVR2* exon 3 OF M1 cells (the main peak is A_8) (Fig. 2). These data indicate that the M1 population of *hMLH1*$^{-/-}$ *ACVR2* exon 10 OF cells has a higher tendency for −1bp frameshift mutation than *hMLH1*$^{-/-}$ *ACVR2* exon 3 OF cells and only *hMLH1*$^{-/-}$ *ACVR2* exon 10 OF cells complete the mutation process into an M2 population. The M1 population from *hMSH6*$^{-/-}$ *ACVR2* exon 10 OF cells revealed WT microsatellite sequence, although its M2 population revealed the mutant sequence, and suggests a lower tendency for

heterodulpex formation in the *hMSH6*$^{-/-}$ background compared to the *hMLH1*$^{-/-}$ background.

As we observed previously (Chung et al., 2008), The −1 bp mutation frequency of the M2 population from the *ACVR2* exon 10 sequence in the *hMLH1*$^{-/-}$ background dramatically accumulated over time whereas one of its M1 population showed little change over time (Fig. 3), again indicating that M1 and M2 are distinct populations. In the M1 population, mutation frequency of *hMLH1*$^{-/-}$ *ACVR2* exon 10 cells was higher than other cell lines and increased over time (highest at day 28, 12-fold change), although the increase over time was small when compared to the increase in the M2 population (Fig. 3A). There was no consistent increase in the M1 population in other cell lines. Only the *ACVR2* exon 10 sequence in *hMLH1*$^{-/-}$ and *hMSH6*$^{-/-}$ backgrounds revealed any prominent M2 population. In the M2 population, *ACVR2* exon 10 sequence in the *hMLH1*$^{-/-}$ background showed its highest mutation frequency over time (up to day 21, 143-fold change) as predicted by the EGFP histograms (Fig. 1) and mutation frequency of the *ACVR2* exon 10 sequence in the *hMSH6*$^{-/-}$ background also increased over time showing its highest mutation frequency on day 28 (5-fold change), although this frequency is much lower than the one of *ACVR2* exon 10 sequence in *hMLH1*$^{-/-}$ cells (Fig. 3B). In *hMLH1*$^{-/-}$ ACVR2 exon 3 cells, *hMSH6*$^{-/-}$ ACVR2 exon 3 cells, and all *hMSH3*$^{-/-}$ cell lines, M2 cells were extremely rare events (average 0.002%) at all time points, with no significant difference in numbers of the M2 population between MR *ACVR2* OF and *ACVR2* OF cells, as shown in Fig. 1. Thus, fold changes in the M2 population of these cells were 1 at all time points (Fig. 3B).

The M2 population (full mutants) was used to calculate the mutation rates. The mutation rate of *ACVR2* exon 10 microsatellite in *hMLH1* deficiency was $1.61 \times 10^{-4} \pm 0.49 \times 10^{-4}$. The mutation rate at the microsatellite of *ACVR2* exon 10 in *hMSH6* deficiency ($0.15 \times 10^{-4} \pm 0.02 \times 10^{-4}$) is ~10 times lower than one in *hMLH1* deficiency. These mutation rates are comparable to ones determined previously (Chung et al., 2008). Mutation rates from *hMSH3*$^{-/-}$ *ACVR2* exon 10 cells and all cell lines containing *ACVR2* exon 3 sequences were not calculated due to a lack of M2 populations.

Overall, our data indicate that MMR deficient backgrounds determine the mutation frequency and rate of the coding microsatellites of *ACVR2* exon 10 and 3. *hMLH1* deficiency provides the highest susceptibility for frameshift mutation at the microsatellites of both exons 10 and 3 of *ACVR2* among 3 different MMR deficiencies (*hMLH1*$^{-/-}$, *hMSH6*$^{-/-}$ and *hMSH3*$^{-/-}$). Additionally, the microsatellite of *ACVR2* exon 10 has a higher susceptibility to a −1 bp frameshift mutation than that of *ACVR2* exon 3 in *hMLH1* and *hMSH6* deficiencies, showing exonic selectivity for a −1 bp frameshift mutation of *ACVR2*, which is observed in CRC with MSI.

Flanking sequences of *ACVR2* microsatellites modify heteroduplex formation and frameshift mutation rates in the *hMLH1* $^{-/-}$ background

To address the cause of the exonic selectivity for a −1bp frameshift mutation of *ACVR2* in MMR deficiency, we hypothesized that the different mutation rates for each coding microsatellite of *ACVR2* could be determined by DNA sequences surrounding the microsatellite. To test this, stable cell lines containing substituted *ACVR2* sequences (Table

1), *hMLH1⁻/⁻* MR *ACVR2* exon 10-exon 3 F IF, *ACVR2* exon 10-exon 3 F OF, MR *ACVR2* exon 3-exon 10 F IF, and *ACVR2* exon 3-exon 10 F OF cells were generated. Previously generated *hMLH1⁻/⁻* stable cell lines containing the native *ACVR2* sequences (Table S1) were used together for comparison of EGFP expression between native and substituted *ACVR*2 sequences.

To compare mutation frequencies and rates of cells containing native *ACVR*2 exon 10 and 3 sequences with ones of cells containing substituted *ACVR*2 exon 10 and 3 sequences in the *hMLH1⁻/⁻* background, non-fluorescent cells containing either MR *ACVR2* exon 10 OF, *ACVR2* exon 10 OF, *ACVR2* exon 10-exon 3 F OF, MR *ACVR2* exon 3 OF, *ACVR2* exon 3 OF or *ACVR2* exon 3-exon 10 F OF were sorted and exponentially grown for 14 to 35 days. EGFP histograms at day 28 were shown in Fig. 4. Consistent with earlier results, in this independent experiment *hMLH1⁻/⁻ ACVR2* exon 3 OF cells revealed only the M1 population whereas *hMLH1⁻/⁻ ACVR2* exon 10 OF cells revealed both M1 and M2 populations. The *ACVR2* exon 10 microsatellite with exon 3 flanking sequences (*ACVR2* exon 10-exon 3 F OF) showed a 2.6-fold less M1 and 24-fold less M2 populations compared to cells containing native *ACVR2* exon 10 OF sequence. In comparison, cells containing *ACVR2* exon 3-exon 10 F OF sequence had a 1.5-fold higher M1 population than the cells containing native *ACVR2* exon 3 OF sequence. Furthermore, a new M2 population developed in cells containing *ACVR2* exon 3-exon 10 F OF sequence that was completely absent in *hMLH1⁻/⁻ ACVR2* exon 3 OF cells. These data indicate that the surrounding sequences of *ACVR2* microsatellite alter −1 bp frameshift mutation frequencies in the *hMLH1* deficiency.

The −1 bp mutation frequency at each time point was shown in Fig. 5. For the M1 population in this independent experiment, the mutation frequency for *hMLH1⁻/⁻ ACVR2* exon 10 OF cells was higher than other cell lines at all time points and increased up to day 21 (28-fold) and then decreased (Fig. 5). This is consistent in pattern and extent with our earlier results. The M1 population of *hMLH1⁻/⁻ ACVR2* exon 10-exon 3 F OF, *ACVR2* exon 3-exon 10 F OF, and *ACVR2* exon 3 OF cells showed ~5–20 times less mutation frequency compared to *hMLH1⁻/⁻ ACVR2* exon 10 OF cells, but showed steady-state stable increases in frequency over time. For the M2 population, *hMLH1⁻/⁻ ACVR2* exon 10 OF cells demonstrated the highest mutation frequency over time compared to other cell lines, as predicted in EGFP histograms (Fig. 4). As observed previously (Chung et al., 2008) and in our earlier results, the M2 population in this independent experiment from *hMLH1⁻/⁻ ACVR2* exon 10 OF cells accumulated over time. A significantly decreased mutation frequency ($P<0.01$) was observed in the M2 population of *hMLH1⁻/⁻ ACVR2* exon 10-exon 3 F OF cells at all time points compared to *hMLH1⁻/⁻ ACVR2* exon 10-OF cells (Fig. 5). *hMLH1⁻/⁻ ACVR2* exon 3 cells did not reveal an M2 population, whereas *hMLH1⁻/⁻ ACVR2* exon 3- exon 10 F OF cells revealed small proportions of an M2 population at day 28 (3-fold change) and day 35 (4-fold change). However, there is no significant difference between the mutation frequencies of *hMLH1⁻/⁻ ACVR2* exon 10-exon 3 F OF and *hMLH1⁻/⁻ ACVR2* exon 3-exon 10 F OF cells at all time points.

To confirm that our EGFP expression experiments resulted in frameshifts, at day 21 after being plated as non-fluorescent cells, the M1 and/or M2 cell populations of *hMLH1⁻/⁻* MR

ACVR2 exon 10 OF, *ACVR2* exon 10 OF, *ACVR2* exon 10-exon 3 F OF, MR *ACVR2* exon 3 OF, *ACVR2* exon 3 OF, or *ACVR2* exon 3-exon 10 F OF cells were sorted and expanded for sequencing analysis. Single cell clones were individually sequenced to assess for frameshift mutation. As expected, nearly all DNA clones (90–100%) from the M2 population of cell lines containing *ACVR2* exon 10 OF or *ACVR2* exon 10-exon 3 F OF revealed −1 bp frameshifts (A_7) (Table 2), indicating full mutant (A_7/T_7) formation. The M2 population of *hMLH1*$^{−/−}$ *ACVR2* exon 3-exon 10 F OF cells did not commence until day 28 after plating, and thus sequencing analysis for the M2 population of this cell line was not performed. On the other hand, DNA clones from the M1 population of *hMLH1*$^{−/−}$ *ACVR2* exon 10 OF and *ACVR2* exon 10-exon 3 F OF revealed 74 and 55% of mutant microsatellite and 26 and 45% of WT microsatellite, respectively (Table 2), indicating heteroduplex (A_8/T_7) formation. Swapping the surrounding DNA sequences of the *ACVR2* exon 10 microsatellite with ones surrounding the *ACVR2* exon 3 microsatellite decreased the number of clones with mutant microsatellites from 74 to 55% for the M1 population. In comparison, DNA clones from the M1 population of *hMLH1*$^{−/−}$ *ACVR2* exon 3 OF and *ACVR2* exon 3-exon 10 F OF cells increased from 47 to 90% of mutant microsatellites, respectively, indicating that the exon 10 flanking sequences allow a microsatellite to be more prone to mutation with DNA MMR deficiency (Table 2). These sequencing data demonstrate that the flanking sequences of *ACVR2* microsatellite alter heteroduplex formation in the *hMLH1*$^{−/−}$ background.

As shown in Table 3, the mutation rate for *hMLH1*$^{−/−}$ *ACVR2* exon 10 cells was $4.37 \times 10^{-5} \pm 0.49 \times 10^{-5}$. The mutation rate for *hMLH1*$^{−/−}$ *ACVR2* exon 10- exon 3 F OF cells ($0.67 \times 10^{-5} \pm 0.37 \times 10^{-5}$) is ~6 times lower compared to counterpart cells containing *ACVR2* exon 10 OF sequence ($P < 0.001$) indicating that the exon 3 flanking sequences make a microsatellite less prone to mutation with DNA MMR deficiency. The mutation rate from *hMLH1*$^{−/−}$ *ACVR2* exon 3 cells was 0.00×10^{-5}, as no M2 population developed over 35 days of observation. However, cells containing *ACVR2* exon 3-exon 10 F OF sequence revealed a new M2 population at day 28, with a mutation rate of $0.93 \times 10^{-5} \pm 0.51 \times 10^{-5}$. These data indicate that the surrounding sequences of *ACVR2* microstellites alter mutation rates of the two *ACVR2* coding microsatellites in the *hMLH1*$^{−/−}$ background.

DISCUSSION

In this study, we hypothesized that the different frameshift mutation frequencies of the coding microsatellites of *ACVR2* exon 10 and 3 in CRC with MSI are determined by DNA sequences flanking the microsatellites. To test this, we utilized stable human MMR cell lines in which we transfected *ACVR2* exon 10 and 3 sequences linked out of frame to EGFP (Chung et al., 2008), and these cell lines allowed us to observe mutations occurring in real time. We first show the selectivity for *ACVR2* exon 10 frameshift mutation over *ACVR2* exon 3 in MMR deficiency using our model. Indeed, as observed in CRC with MSI, only *ACVR2* exon 10 frameshift mutation occurred, with none for *ACVR2* exon 3 (M2 population) in both *hMLH1*$^{−/−}$ and *hMSH6*$^{−/−}$ cells, with neither sequence forming mutations in *hMSH3*$^{−/−}$ cells. The *ACVR2* exon 10 frameshift mutation rate is highest in *hMLH1*$^{−/−}$ cells, which is 10-fold higher than the mutation rate observed for *hMSH6*$^{−/−}$ cells. Thus, our human model is consistent with the selectivity observed for CRC, and as we previously described for our observations between mutation for *TGFBR2* and *ACVR2*

(Chung et al., 2008). Here, a clear selectivity exists for mutation of *ACVR2* exon 10, whereas *ACVR2* exon 3 is relatively protected from frameshift mutation even when DNA MMR function is absent. This dichotomy is remarkable between the two identical length coding microsatellites and perhaps even more remarkable when examining the microsatellites in our model out of the context of the tertiary DNA structure.

We swapped the 5′ and 3′ flanking nucleotides of the *ACVR2* exon 10 microsatellite for the ones surrounding the *ACVR2* exon 3 microsatellite, and visa versa. These constructs were transfected into *hMLH1*$^{-/-}$ cells, which show the highest mutation rate for the WT *ACVR2* exon 10 microsatellite, and simulates sporadic MSI CRC which contain inactivated *hMLH1* by promoter hypermethylation. Here, exon 3 flanking sequences that newly surround the *ACVR2* exon 10 microsatellite slow the mutation rate by 6-fold (Table 3), and greatly diminish the accumulation of full mutant (M2) cells (Fig. 5). In the opposing direction, exon 10 flanking sequences that newly surround *ACVR2* exon 3 microsatellite allow the new completion of full mutant cells, a feat that the WT *ACVR2* exon 3 flanking sequences do not allow at the *ACVR2* exon 3 microsatellite. Thus, the sequence context of the *ACVR2* coding microsatellites influences their mutation rates. Why this occurs is not clear. It has been previously suggested in yeast MMR that base pairs as far away as 15–18 nucleotides could affect mispair recognition, and that footprinting studies of yeast MSH2-MSH6 indicate that these proteins interact with DNA over a region of 25 nucleotides surrounding a mispair (Harrington & Kolodner, 2007; Marsischky & Kolodner, 1999). Thus, the flanking sequences surrounding a DNA mismatch repairable target could affect the stability of the MMR protein-DNA interaction. This aspect could be tested by studying binding interactions between the human MMR proteins and DNA. Other hypotheses for affecting frameshift mutation include: strength of Watson-Crick hydrogen bonding around a mispair or IDLs, and the nature of the secondary structure of DNA. In our experiments, certainly the primary DNA structure helps dictate mutability of the *ACVR2* microsatellites in the absence of DNA MMR.

The establishment of our human model allowed us to clearly observe the occurrence of pass-through heteroduplexes (the M1 population), prior to full mutants (the M2 population). However, heteroduplex formation does not necessarily mean mutation is imminent, as either repair can occur, or the flanking sequences surrounding a microsatellite may prevent full mutation, and our data bear that out. Both *ACVR2* exon 10 and 3 microsatellites developed an M1 heteroduplex population in *hMLH1*$^{-/-}$ cells, but only the *ACVR2* exon 10 microsatellite fully mutated. Cloned sequences from *hMLH1*$^{-/-}$ *ACVR2* exon 3 cells revealed a nearly even split between A_7 and A_8 sequences, very indicative of heteroduplex formation, and which occurred at a slow and steady rate but did not lead to a M2 population. When the flanking sequences from *ACVR2* exon 10 microsatellite were placed around the *ACVR2* exon 3 microsatellite, heteroduplex formation increased, and corresponded to the new observation of a M2 population. Additionally, when the flanking sequences from *ACVR2* exon 3 microsatellite were placed around the *ACVR2* exon 10 microsatellite, heteroduplex formation slowed and corresponded to a reduction in the subsequent M2 population. Thus, the flanking sequences alter heteroduplex formation at microsatellite, which determines its ability to become fully frameshifted in the setting of defective MMR.

There are several genes containing coding microsatellites that potentially can be mutated in the setting of DNA MMR deficiency. However, analysis of tumors or cell lines indicates that the mutation frequencies vary widely between genes, even for coding microsatellites of the same length (Hempen et al., 2003; Jung et al., 2004). Additionally, some genes that show some degree of frameshift mutation have not been fully demonstrated that mutation has biological consequences. *ACVR2*, for example, has been demonstrated to be frameshift mutated, and lose protein expression and tumor suppressor capability in colorectal cancer (Jung et al., 2004; Jung et al., 2007). This study sheds a possible explanation why certain genes may become frameshift mutated in the setting of defective MMR, while others do not, although it does not address subsequent biological functional consequences.

In summary, we demonstrate frameshift mutation selectivity for the *ACVR2* exon 10 over the *ACVR2* exon 3 microsatellite in human colorectal cells with MMR deficiency in real time. We also demonstrate that this selectivity for frameshift mutation within *ACVR2* lies in part with the flanking nucleotides surrounding each microsatellite. Our study has implication for the occurrence of frameshift mutation at other microsatellite sequences and for how MMR deficiency drives frameshift mutation.

Supplementary Material

Refer to Web version on PubMed Central for supplementary material.

Acknowledgments

Abbreviations

|	
TGFBR2	transforming growth factor β receptor 2
ACVR2	activin type II receptor
MMR	mismatch repair system
MSI	microsatellite instability
IDL	insertion deletion loop
MR	mutation resistant
IF	in frame of EGFP
OF	+1bp out of frame of EGFP
EGFP	enhanced green fluorescent protein
CRC	colorectal cancer

References

Acharya S, Wilson T, Gradia S, Kane MF, Guerrette S, Marsischky GT, et al. hMSH2 forms specific mispair-binding complexes with hMSH3 and hMSH6. Proc Natl Acad Sci U S A. 1996; 93:13629–34. [PubMed: 8942985]

Akiyama Y, Sato H, Yamada T, Nagasaki H, Tsuchiya A, Abe R, et al. Germ-line mutation of the hMSH6/GTBP gene in an atypical hereditary nonpolyposis colorectal cancer kindred. Cancer Res. 1997; 57:3920–3. [PubMed: 9307272]

Carethers JM, Chauhan DP, Fink D, Nebel S, Bresalier RS, Howell SB, et al. Mismatch repair proficiency and in vitro response to 5-fluorouracil. Gastroenterology. 1999; 117:123–31. [PubMed: 10381918]

Chung H, Young DJ, Lopez CG, Le TA, Lee JK, Ream-Robinson D, et al. Mutation rates of TGFBR2 and ACVR2 coding microsatellites in human cells with defective DNA mismatch repair. PLoS ONE. 2008; 3:e3463. [PubMed: 18941508]

Fishel R, Lescoe MK, Rao MR, Copeland NG, Jenkins NA, Garber J, et al. The human mutator gene homolog MSH2 and its association with hereditary nonpolyposis colon cancer. Cell. 1993; 75:1027–38. [PubMed: 8252616]

Grady WM, Carethers JM. Genomic and epigenetic instability in colorectal cancer pathogenesis. Gastroenterology. 2008; 135:1079–99. [PubMed: 18773902]

Harrington JM, Kolodner RD. Saccharomyces cerevisiae Msh2-Msh3 acts in repair of base-base mispairs. Mol Cell Biol. 2007; 27:6546–54. [PubMed: 17636021]

Hempen PM, Zhang L, Bansal RK, Iacobuzio-Donahue CA, Murphy KM, Maitra A, et al. Evidence of selection for clones having genetic inactivation of the activin A type II receptor (ACVR2) gene in gastrointestinal cancers. Cancer Res. 2003; 63:994–9. [PubMed: 12615714]

Herman JG, Umar A, Polyak K, Graff JR, Ahuja N, Issa JP, et al. Incidence and functional consequences of hMLH1 promoter hypermethylation in colorectal carcinoma. Proc Natl Acad Sci U S A. 1998; 95:6870–5. [PubMed: 9618505]

Jung B, Doctolero RT, Tajima A, Nguyen AK, Keku T, Sandler RS, et al. Loss of activin receptor type 2 protein expression in microsatellite unstable colon cancers. Gastroenterology. 2004; 126:654–9. [PubMed: 14988818]

Jung B, Smith EJ, Doctolero RT, Gervaz P, Alonso JC, Miyai K, et al. Influence of target gene mutations on survival, stage and histology in sporadic microsatellite unstable colon cancers. Int J Cancer. 2006; 118:2509–13. [PubMed: 16380996]

Jung BH, Beck SE, Cabral J, Chau E, Cabrera BL, Fiorino A, et al. Activin type 2 receptor restoration in MSI-H colon cancer suppresses growth and enhances migration with activin. Gastroenterology. 2007; 132:633–44. [PubMed: 17258738]

Luria SE, Delbruck M. Mutations of Bacteria from Virus Sensitivity to Virus Resistance. Genetics. 1943; 28:491–511. [PubMed: 17247100]

Markowitz S, Wang J, Myeroff L, Parsons R, Sun L, Lutterbaugh J, et al. Inactivation of the type II TGF-beta receptor in colon cancer cells with microsatellite instability. Science. 1995; 268:1336–8. [PubMed: 7761852]

Marsischky GT, Kolodner RD. Biochemical characterization of the interaction between the Saccharomyces cerevisiae MSH2-MSH6 complex and mispaired bases in DNA. J Biol Chem. 1999; 274:26668–82. [PubMed: 10480869]

Modrich P. Mechanisms in eukaryotic mismatch repair. J Biol Chem. 2006; 281:30305–9. [PubMed: 16905530]

Nicolaides NC, Papadopoulos N, Liu B, Wei YF, Carter KC, Ruben SM, et al. Mutations of two PMS homologues in hereditary nonpolyposis colon cancer. Nature. 1994; 371:75–80. [PubMed: 8072530]

Palombo F, Iaccarino I, Nakajima E, Ikejima M, Shimada T, Jiricny J. hMutSbeta, a heterodimer of hMSH2 and hMSH3, binds to insertion/deletion loops in DNA. Curr Biol. 1996; 6:1181–4. [PubMed: 8805365]

Papadopoulos N, Nicolaides NC, Wei YF, Ruben SM, Carter KC, Rosen CA, et al. Mutation of a mutL homolog in hereditary colon cancer. Science. 1994; 263:1625–9. [PubMed: 8128251]

Parsons R, Myeroff LL, Liu B, Willson JK, Markowitz SD, Kinzler KW, et al. Microsatellite instability and mutations of the transforming growth factor beta type II receptor gene in colorectal cancer. Cancer Res. 1995; 55:5548–50. [PubMed: 7585632]

Thibodeau SN, Bren G, Schaid D. Microsatellite instability in cancer of the proximal colon. Science. 1993; 260:816–9. [PubMed: 8484122]

Veigl ML, Kasturi L, Olechnowicz J, Ma AH, Lutterbaugh JD, Periyasamy S, et al. Biallelic inactivation of hMLH1 by epigenetic gene silencing, a novel mechanism causing human MSI cancers. Proc Natl Acad Sci U S A. 1998; 95:8698–702. [PubMed: 9671741]

Woerner SM, Kloor M, Mueller A, Rueschoff J, Friedrichs N, Buettner R, et al. Microsatellite instability of selective target genes in HNPCC-associated colon adenomas. Oncogene. 2005; 24:2525–35. [PubMed: 15735733]
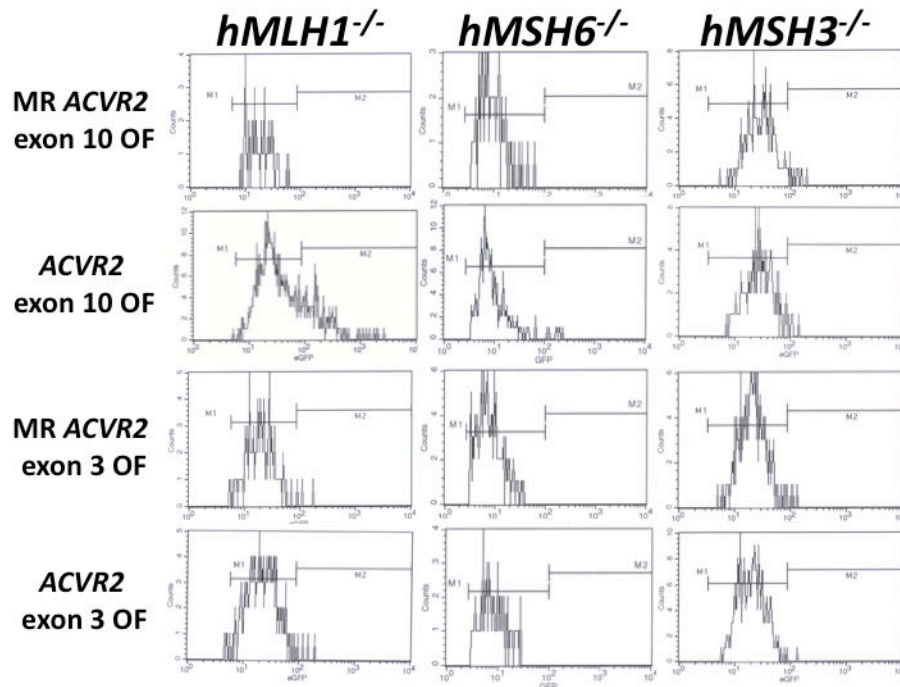
Figure 1. Mutation analysis of cells containing native *ACVR2* exon 10 or exon 3 sequences by flow cytometry

Non-fluorescent cells were sorted and exponentially grown for 7 to 28 days. At specific time points, cells were harvested, and 200,000 cells were analyzed for EGFP expression (identifying a −1bp frameshift mutation) by flow cytometry. Gated live cells were analyzed on an EGFP histogram and two distinct EGFP populations were plotted. The population with dim EGFP expression was designated M1 and the population with bright EGFP expression was designated M2. EGFP histograms of MR *ACVR2* exon 10 OF, *ACVR2* exon 10 OF, MR *ACVR2* exon 3 OF, and *ACVR2* exon 3 OF cells in different MMR deficient backgrounds at day 21 were shown as representatives of mutation analysis. Note that scaling of cell counts in each EGFP histogram is different.
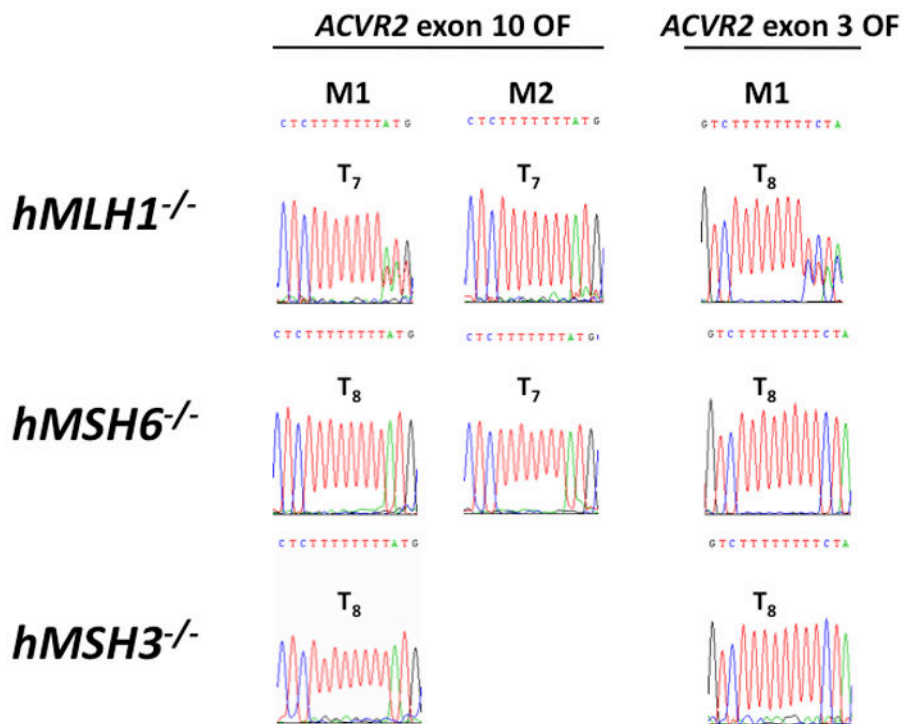
Figure 2. Sequences demonstrating frameshift mutation of *ACVR2* exon 10 and *ACVR2* exon 3 in different human MMR-deficient backgrounds

Cells from the M1 and/or M2 populations of *ACVR2* exon 10 OF and *ACVR2* exon 3 OF cells in different MMR deficient backgrounds ($hMLH1^{-/-}$, $hMSH6^{-/-}$, and $hMSH3^{-/-}$) were sorted and cultured for DNA sequencing analysis. DNA from each cell line was amplified by PCR and anti-sense strand was sequenced to assess for frameshift mutation of the coding microsatellites of *ACVR2* exon 10 and *ACVR2* exon 3. The M1 population of $hMLH1^{-/-}$ *ACVR2* exon 10 OF cells revealed overlapped sequences from mutant (T_7) and WT microsatellites (T_8) (with the mutant sequence as dominant), indicating heteroduplex formation whereas the M2 populations containing *ACVR2* exon 10 OF sequence revealed only mutant microsatellite sequences in both $hMLH1^{-/-}$ and $hMSH6^{-/-}$ backgrounds, indicating full mutant formation. On the other hand, *ACVR2* exon 3 OF sequence did not show a full mutant microsatellite sequence (M2 population) in any human MMR deficient backgrounds although its M1 population revealed a mixture of WT (T_8) and mutant (T_7) sequences (with the WT sequence as dominant) in the $hMLH1^{-/-}$ background. The M1 population from all MR OF cells, $hMSH6^{-/-}$ and $hMSH3^{-/-}$ cells containing *ACVR2* exon 10 or exon 3 OF did not show any frameshift mutation.
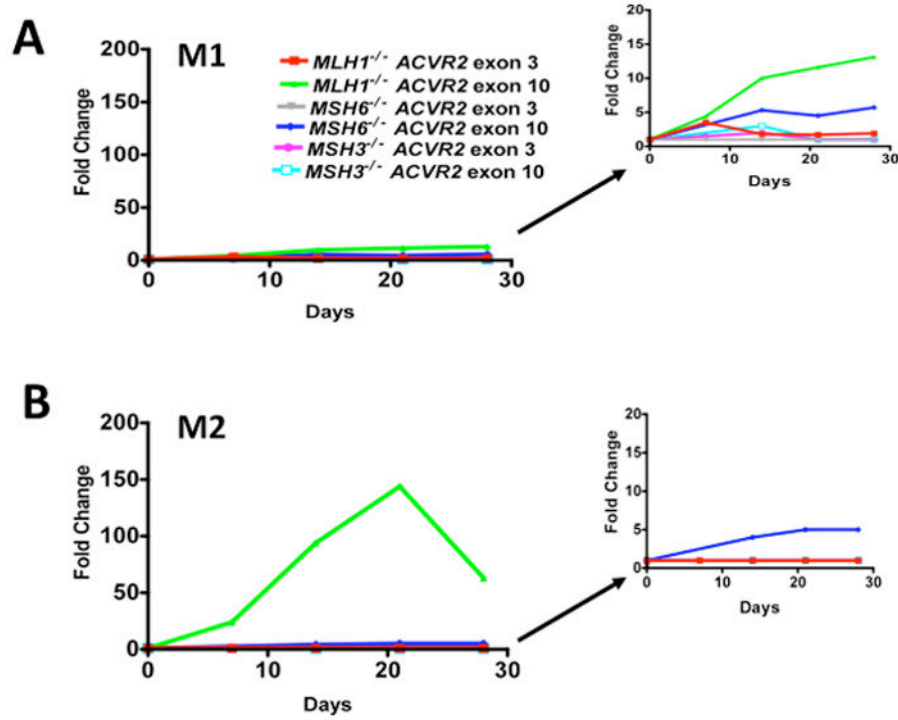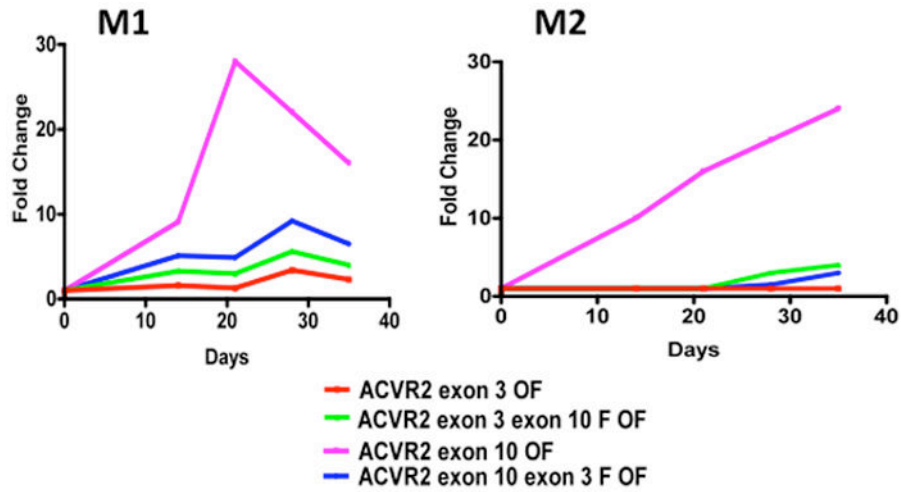
Figure 3. Mutation frequencies of *ACVR2* exon 10 and *ACVR2* exon 3 in different MMR backgrounds

Non-fluorescent cells were analyzed for EGFP expression by flow cytometry at 7, 14, 21, and 28 days after being sorted and cultured. EGFP analysis was performed at each day as shown in Fig. 1. Mutation frequency at each time point was expressed as a fold change using the following formula: (EGFP positive cells/total live cells from *ACVR2* OF cells)/(EGFP positive cells/total live cells from MR *ACVR2* OF cells). Only the *ACVR2* exon 10 sequence in *hMLH1*−/− and *hMSH6*−/− cells revealed the M2 (full mutant) population. *ACVR2* exon 10 sequence in the *hMLH1*−/− background showed the highest mutation frequency for both M1 and M2 populations accumulating over time. The M1 populations of *ACVR2* exon 10 sequence in the different MMR-deficient backgrounds and the *ACVR2* exon 3 sequence in all MMR deficient backgrounds did not show any consistent increase in mutation frequency over time. The M2 population of *ACVR2* exon 10 sequence in the *hMSH6*−/− background had a slight increase in mutation frequency over time, although this frequency is much lower than one of *ACVR2* exon 10 sequence in the *hMLH1*−/− background. Cell lines showing lower mutation frequencies (less than 20-fold change) were separately plotted in the right panel using a smaller y-axis scale. Data are means from two independent experiments at each time point.
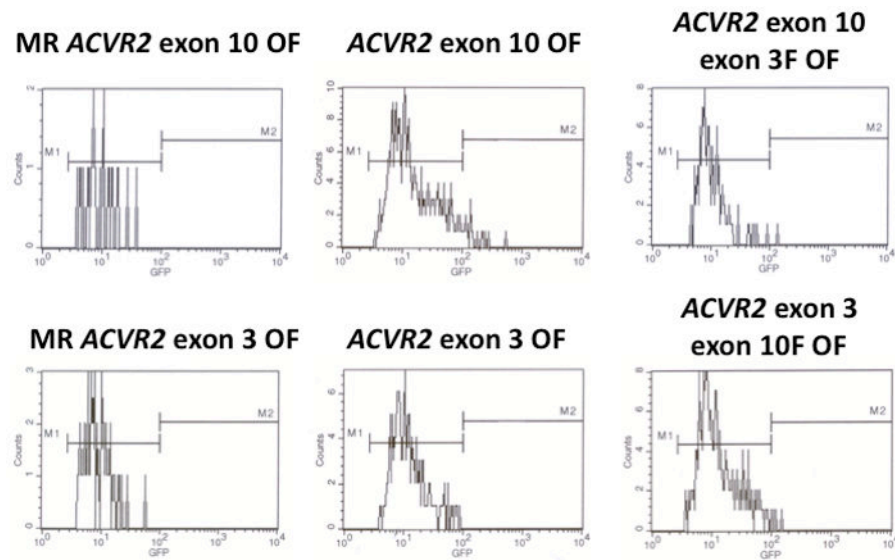
Figure 4. Mutation analysis of cells containing substituted *ACVR2* exons 10 or 3 sequences by flow cytometry

Non-fluorescent cells were sorted and exponentially grown for 14 to 35 days. At specific time points, cells were harvested, and analyzed for EGFP expression by flow cytometry as described in Fig. 1. EGFP histograms of MR *ACVR2* exon 10 OF, *ACVR2* exon 10 OF, *ACVR2* exon 10-exon 3 F OF, MR *ACVR2* exon 3 OF, *ACVR2* exon 3 OF, *ACVR2* exon 3-exon 10 F OF cells in the *hMLH1*$^{-/-}$ background at day 28 were shown as representatives of mutation analysis. Scaling of cell counts for each EGFP histogram is different.

Figure 5. Mutation frequencies of native and substituted *ACVR2* exons 10 and 3 sequences in the *hMLH1*$^{-/-}$ background

Non-fluorescent cells were analyzed for EGFP expression by flow cytometry at 14, 21, 28, and 35 days after being sorted and cultured, and EGFP analysis was performed at each day as shown in Fig. 4. Mutation frequency at each time point was determined as described in Fig. 3. In the M1 population, *hMLH1*$^{-/-}$ *ACVR2* exon 10 OF cells showed the highest mutation frequency followed by *hMLH1*$^{-/-}$ *ACVR2* exon 10-exon 3F OF, *hMLH1*$^{-/-}$ *ACVR2* exon 3- exon 10F OF, and *hMLH1*$^{-/-}$ *ACVR2* exon 3 OF cells at all time points. The M2 population of *hMLH1*$^{-/-}$ *ACVR2* exon 10 OF cells revealed the highest mutation frequency over time compared to other cell lines. Significantly decreased mutation frequency was observed in the M2 population of *hMLH1*$^{-/-}$ *ACVR2* exon 10-exon 3F OF cells compared to cells containing native *ACVR2* exon 10 OF sequence. No full mutant M2 population was observed in *hMLH1* $^{-/-}$ *ACVR2* exon 3 cells whereas *hMLH1*$^{-/-}$ *ACVR2* exon 3-exon 10 F OF cells revealed its M2 population from day 28. Data are means from two independent experiments at each time point.

Table 1

Sequences of exon 10 and exon 3 of *ACVR2* used for cloning into pIREShyg2-EGFP plasmid.

ACVR2 plasmids	*ACVR2* sequences
MR *ACVR2* exon 10 IF	GACCTGTAGATGAATACATGTTGCCATTTGAGGAGGAAATTGGCCAGCATCCATCTCTTGAAGACATGCAGGAAGTTGTTGTGTGCATAAAGAGAAAAAGAGGGCCTGTTT
MR *ACVR2* exon 10 OF	GACCTGTAGATGAATACATGTTGCCATTTGAGGAGGAAATTGGCCAGCATCCATCTCTTGAAGACATGCAGGAAGTTGTTGTGTGCATAAAGAGAAAAAGAGGGCCTGTTTT
ACVR2 exon 10 OF	GACCTGTAGATGAATACATGTTGCCATTTGAGGAGGAAATTGGCCAGCATCCATCTCTTGAAGACATGCAGGAAGTTGTTGTGTGCATAAAAAAAAGAGGGCCTGTTTT
MR *ACVR2* exon 3 IF	CTCTGCTTATTTATAGGACTGATTGTGTAGAAAAGAAAGACAGCCCTGAAGTATATT
MR *ACVR2* exon 3 OF	CTCTGCTTATTTATAGGACTGATTGTGTAGAAAAGAAAGACAGCCCTGAAGTATATTT
ACVR2 exon 3 OF	CTCTGCTTATTTATAGGACTGATTGTGTAGAAAAAAAGACAGCCCTGAAGTATATTT
MR *ACVR2* exon 10-exon 3 F IF	GACCTGTAGATGAATACATGTTGCCATTTG AGGAGGAAATTGGCCAGCATCCATCTCTTGAAGACATGCAGGAAGTTGT*TGTGT*ATAAAGAGAAAAAGA*CAGC*TGTTT
ACVR2 exon 10-exon 3 F OF	GACCTGTAGATGAATACATGTTGCCATTTG AGGAGGAAATTGGCCAGCATCCATCTCTTGAAGACATGCAGGAAGTTGT*TGTGT*ATAAAAAAAGA*CAGC*TGTTT
MR *ACVR2* exon 3-exon 10 F OF	CTCTGCTTATTTATAGGACTGAT*TGTGCA*GAAAAGAAAGA*GGGC*CCCTGAAGTATATT
ACVR2 exon 3-exon 10 F OF	CTCTGCTTATTTATAGGACTGAT*TGTGCA*GAAAAAAAGA*GGGC*CCCTGAAGTATATTT

Various exon 10 or exon 3 of *ACVR2* sequences were inserted immediately after the translation initiation codon of EGFP gene being in frame of the EGFP gene (IF) or +1 bp out of reading frame of the EGFP gene (OF) in pIRES hyg2-EGFP plasmid (Fig. S1). Mutation resistant (MR) plasmids were constructed by interrupting microsatellite sequences (A8 to A3GA4). MR IF and MR OF plasmids were used for positive and negative controls for EGFP expression, respectively. OF plasmids are the experimental plasmids. Six nucleotides (presented in *italic*) flanking *ACVR2* exons 10 or 3 microsatellites on the 5′ and 3′ ends were replaced with the 6 nucleotides (presented in *italic*) flanking exons 3 or 10 microsatellites to construct *ACVR2* exon 10-exon 3 F and *ACVR2* exon 3-exon 10 F plasmids, respectively. The first nucleotides (T for exon 10 and G for exon 3) flanking 5′ of the exon 10 or 3 microsatellites were not substituted to avoid generation of a new in-frame stop codon which would interrupt mutation analysis by EGFP expression. With these substituted sequences, MR IF and OF plasmids were constructed. Each substituted sequence had net 4 nucleotide changes (labeled in *italic* and bold letters) compared to WT sequence.

Table 2

Frameshift mutation at the coding microsatellites of *ACVR2* exon 10 and *ACVR2* exon 3 in native and substituted *ACVR2* sequences in the *hMLH1* $^{-/-}$ background.

Genes	EGFP intensity	A_7/T_7 clones	A_8/T_8 clones	% mutated
ACVR2 exon10	M1	14	5	74
	M2	18	2	90
ACVR2 exon10-exon 3 F	M1	10	8	55
	M2	20	0	100
ACVR2 exon 3	M1	8	9	47
ACVR2 exon 3-exon 10 F	M1	18	2	90

Cells from the M1 and/or M2 populations of *hMLH1*$^{-/-}$ *ACVR2* exon 10 OF, *ACVR2* exon 10-exon 3 F OF, *ACVR2* exon 3 OF, and *ACVR2* exon 3-exon 10 F OF cells were sorted and cultured. DNA from each cell line was amplified by PCR, sub-cloned and all single cell clones were individually sequenced to assess for frameshift mutation at the coding microsatellite. Most DNA clones from the M2 population of *hMLH1*$^{-/-}$ *ACVR2* exon 10 OF and *hMLH1*$^{-/-}$ *ACVR2* exon 10-exon 3 F OF cells revealed −1 bp frameshift mutation (A7), indicating full mutant (A7/T7) formation. Note that *hMLH1*$^{-/-}$ *ACVR2* exon 10-exon 3 F OF cells showed a decrease in mutant M1 clones compared to *hMLH1*$^{-/-}$ *ACVR2* exon 10 OF cells, whereas *hMLH1*$^{-/-}$ *ACVR2* exon 3-exon 10 F OF cells showed an increase in mutant M1 clones compared to *hMLH1*$^{-/-}$ *ACVR2* exon 3 OF cells, indicating that these flanking sequences alter heteroduplex (A8/T7) formation in the *hMLH1* $^{-/-}$ background.

Table 3

Calculated mutation rates at the coding microsatellites of *ACVR2* exon 10 and *ACVR2* exon 3 in native and substituted *ACVR2* sequences in the *hMLH1*$^{-/-}$ background.

Gene	Microsatellite	Flanking sequence	Rate for mutation
ACVR2 exon 10 OF	Exon 10	Exon10	$4.37 \times 10^{-5} \pm 0.49 \times 10^{-5}$ [*]
ACVR2 exon 10-exon 3 F OF	Exon 10	Exon 3	$0.67 \times 10^{-5} \pm 0.37 \times 10^{-5}$
ACVR2 exon 3 OF	Exon 3	Exon 3	$0.00 \times 10^{-5} \pm 0.00 \times 10^{-5}$
ACVR2 exon 3-exon 10 F OF	Exon 3	Exon 10	$0.93 \times 10^{-5} \pm 0.51 \times 10^{-5}$

Data from the M2 cell populations from each time point between day 21 and day 35 were used for mutation rate analysis. Single mutation rates were calculated by combining and averaging time-specific mutation rates. Data shown are mean ± SEM.

[*] $P<0.001$ comparing *hMLH1*$^{-/-}$ *ACVR2* exon 10 OF cells with each of *hMLH1*$^{-/-}$ *ACVR2* exon 10-exon 3 F OF, *hMLH1*$^{-/-}$ *ACVR2* exon 3 OF, and *hMLH1*$^{-/-}$ *ACVR2* exon 3-exon 10 F OF cells.